ChemComm

Three-dimensional spider-web architecture assembled from Na2Ti3O7 nanotubes as high performance anode for sodium-ion battery

Journal:	*ChemComm*
Manuscript ID:	CC-COM-08-2014-006451.R1
Article Type:	Communication
Date Submitted by the Author:	14-Sep-2014
Complete List of Authors:	Zhang, Yuping; school of chemirsty and enviroment, Beihang university, Guo, Lin; BEIJING UNIVERSITY OF AERONAUTICS & ASTRONAUTICS, Chemistry Yang, Shihe; The Hong Kong University of Science and Technology, Department of Chemistry

Table of content

Spider web-like architecture assembled from $Na_2Ti_3O_7$ nanotubes as high performance anode for Sodium-ion battery

Yuping Zhang, Lin Guo[1], Shihe Yang*[1,2]*

1.School of Chemistry and Environment, Beihang University. Beijing, 100191, P. R. China. E-mail: guolin@buaa.edu.cn

2.Department of Chemistry, The Hong Kong University of Science and Technology, Clear Water Bay, Kowloon Hong Kong (P.R. China). E-mail : chsyang@ust.hk

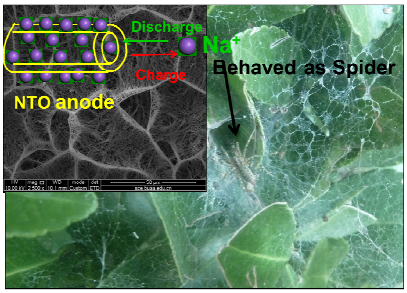

Na inserted/extracted into/from the spider web like architecture assembled by $Na_2Ti_3O_7$ nanotube behave as natural spider feeding on themselves.

Journal Name

RSCPublishing

COMMUNICATION

Three-dimensional spider-web architecture assembled from $Na_2Ti_3O_7$ nanotubes as high performance anode for sodium-ion battery

Cite this: DOI: 10.1039/xoxxoooooox

Received ooth January 2012,
Accepted ooth January 2012

Yuping Zhang,[a] Lin Guo[a]* and Shihe Yang [a,b]*

$Na_2Ti_3O_7$ nanotube-assembled three-dimensional spider-web architecture is synthesized by hydrothermal method. The self-similar network architecture exhibits an excellent performance as an anode for room temperature sodium ion battery without any additives (e.g. binder, conducting agent) for first time.

As a promising alternative to rechargeable lithium-ion batteries, sodium ion batteries have been far less studied due to their much lower energy density. [1] As the technology of lithium-ion battery becomes more and more mature, the research on sodium ion battery has been increasingly brought to the agenda simply because sodium is much more earth abundant than lithium. However, the lower energy density of sodium-ion batteries need be improved to meet the requirement of grid energy storage, [2] so there is still a long way towards commercial realization of sodium-ion batteries, which would be economic, safe, and durable.

Reaching above target for sodium-ion batteries demands finding and optimizing new electrode materials for fast and expedient sodium insertion/extraction and transport. Up till now, most work are concentrated on synthesizing cathode materials with some fruitful results, such as transition metal oxides,[3] poly-anionic compounds,[4] and the transition metal derived Prussian blue analogues [5]. In contrast, the researches over the anode materials for sodium ion batteries is limited. Being much more reactive with organic electrolyte and more prone to dendrite formation during the cycling, the sodium metal used as anode material is much less advisable for battery anode than the lithium metal. Therefore, substitute materials are eagerly replaced sodium metal as anode. As we known well, graphite is commonly used as anode in lithium-ion batteries, but it was not effectively uesd as an anode for sodium-ion battery, because Na^+ ions hardly form staged intercalation compounds with graphite. Many other carbon species, however, such as petroleum-coke carbon [6], carbon black [7], and hard car-bon [8], show promise as anode materials for sodium-ion battery. Recently, $Na_2Ti_3O_7$ (NTO) was also researched as promising negative electrode material [9-12], but the battery performance, especially for the cycling performace, need to be improved, significantly, leaving wide open the opportunities to develop optimal electrode morphologies for the next generation battery electrodes. For many applications ranging from filtration, sensor, drug delivery platform, tissue engineering, etc.,[13] it is desirable to combine one-dimensional (1D) nanostructure and three-dimensional (3D) mesostructure to form certain hierarchical architectures. Such architectures have open porosity, good interconnectivity, and good structural and mechanical compliance and robustness. Not least, these material architectures therefore may also enhance battery performance.[14]

Herein we report a facile route to synthesize a spider web-like $Na_2Ti_3O_7$ material, which is assembled from $Na_2Ti_3O_7$ nanotubes. The nanotubes were directly grown on Ti flake under the alkali hydrothermal condition. When it was utilized as negative electrode without adding any additives (e.g. binder, conducting agent) for room temperature sodium-ion battery for the first time, the spider web-like $Na_2Ti_3O_7$ electrode showed high specific capacity, high rate capability ranging from 450-100 mAh g^{-1} at varied current densities of 0.05-3 A g^{-1}, and long cycling life.

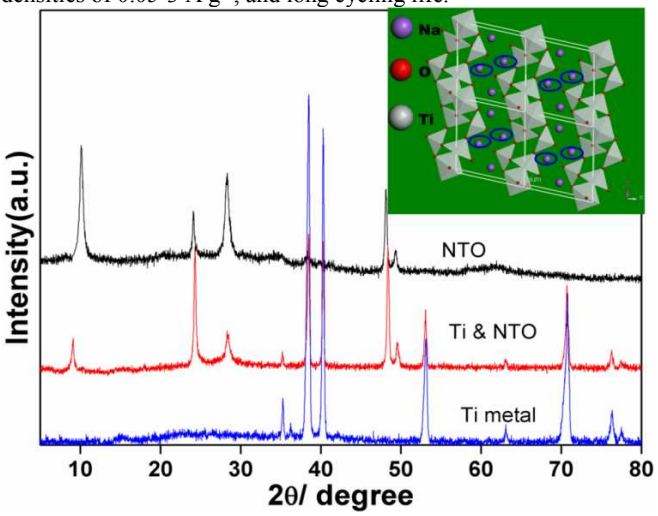

Fig.1 XRD patterns of NTO, NTO on Ti substrate and Ti metal of Ti plate. Top-right inset is crystal structure of NTO.

Fig. 1 shows the XRD patterns of the as prepared NTO, NTO on Ti substrate and titanium metal. The NTO was collected by scrapping from the surface of the substrate. The XRD pattern shows good crystallinity, which is well indexed to the standard XRD trace of $Na_2Ti_3O_7$ (JCPDS no. 31-1329). The crystal structure of NTO is shown in the inset of Fig. 1, in which three edges shared TiO_6 octahedrons are arranged in a zigzag pattern and Na^+ ions are inserted among the TiO_6 layers, and the inserted sodium ions are situated at two different crystallographic sites. The sodium atoms denoted in blue circle bond with oxygen in irregular nine-fold coordination, whereas other sodium atoms without circle mark are

situated in trigonal prisms of oxygen.[15-17] The layer structure formed of the TiO_6 octahedrons provides the space for sodium ions to diffuse or transport easily, which is a principle feature of $Na_2Ti_3O_7$ as electrode for sodium ion battery. As well as XRD characterization, EDX and Raman spectra were also used to identified the existence of $Na_2Ti_3O_7$ as shown in Figure S1 and S2.

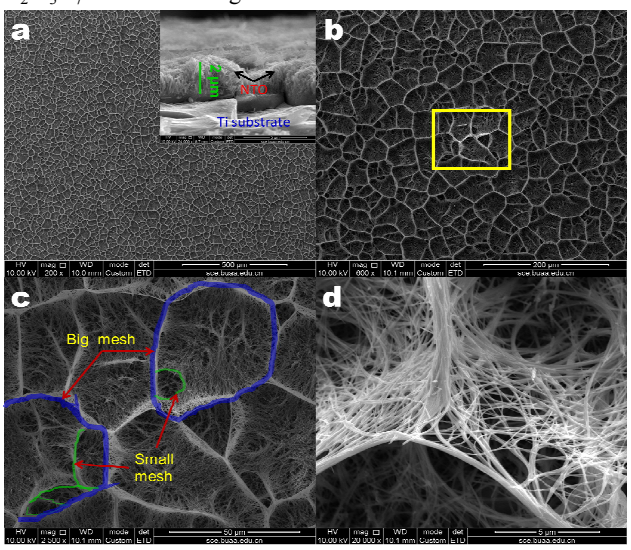

Fig.2 SEM images of the NTO at different magnifications. a) and b): low magnification. c) and d): high magnification of b) in the square. Inset of a) is a fracture surface of NTO.

The field-emission scanning electron microscope (FESEM) images of the NTO are shown in Fig. 2. From the low-magnification FESEM images of Fig. 2a and 2b, irregular shape spider web (natural spider web shown as in Figure S3) with different mesh sizes woven together as a huge meshwork on the substrate of titanium substrate can be clearly seen. Such single big meshes (sketched as blue) are interconnected by longer 1D nanostructure. And even small size meshes (sketched as green) are nested in the holes of the big meshes as shown in Fig. 2c and more clearly seen in Fig. 2d. Close examination shows that the spider webs are assembled from a large number of individual 1D structures, and the tails of these bundles of the 1D nanotubes tangle together acting as the main rim of the mesh. In this way, a 3D spider web like network built up. From Fig. 2c and 2d, the length of 1D unit at ~5 μm or even longer can also be recognized.

To further investigate the building unit of the spider web like $Na_2Ti_3O_7$ structure, TEM and HRTEM images are used to determine the nature of 1D unit, that is, which type of 1D building unit is belong to be? nanowire or nanotube? Fig. 3a is low magnification TEM image of as prepared sample scraped from the Ti substrate. The 1D structure is obviously seen and the length of these 1D structures is range from 1-5 μm. This is a bit different from the length shown in SEM images, because the destruction of 3D spider web structure scraped from the Ti substrate. The longer 1D NTO possibly breaks into smaller ones recurring to external force. Fig. 3b shows that the outer diameters of 1D structure are ca. 50-70 nm, from the inset of Fig. 3b, we can also confirm that 1D structure belongs to nanotube, not nanowire. Moreover, the inner diameter of nanotube is about 10 nm as shown in inset of Fig. 3b, indicating that thick wall of nanotube was formed in the synthesis process. Fig. 3c not only shows us the variational diameter of nanotubes, but also reflects the thick wall of $Na_2Ti_3O_7$ nanotube. Under this resolution, the lattice fringes can be seen from the outside of nanotube wall, and the detail of lattice fringes can be further confirmed to be about 0.84 nm in Fig. 3d, corresponding to the (001) plane spacing of $Na_2Ti_3O_7$ single crystal. In addition, the inset of Fast Fourier-Transform (FFT) pattern in Fig. 3d also confirms the $Na_2Ti_3O_7$ nanotube exposed (001) faces and the angle indicated in the corresponding FFT image is about 63°, which well agrees with the theoretical value for the angle between the (001) and (111) facets. From Both HRTEM images and FFT pattern it is found that the as prepared $Na_2Ti_3O_7$ nanotube mostly exposing its (001) faces, which is also well consistent with it XRD pattern as shown in Fig. 1.

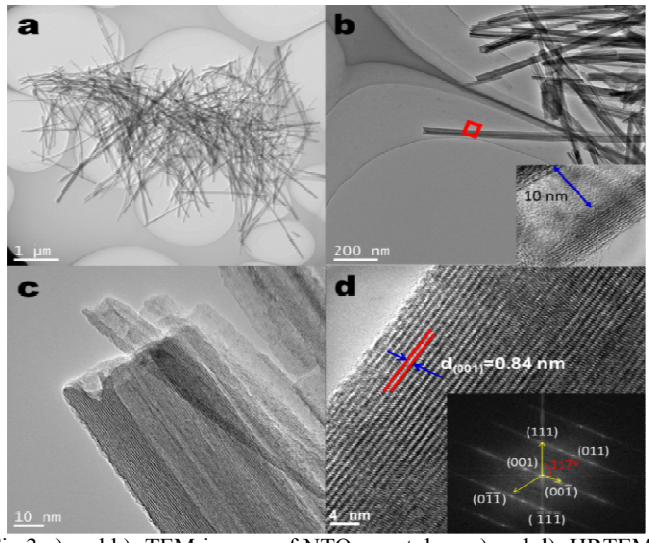

Fig.3 a) and b): TEM images of NTO nanotubes. c) and d): HRTEM images of NTO nanotubes. The inset of b) is HRTEM image of the selected area. The inset of d) is FFT of the TEM image.

Benefitting from this unique structure, the NTO exhibits exceptional electrochemical performance as an anode material in sodium ions battery. Fig.4a shows representative discharge-charge voltage vs specific capacity profile at a current density of 400 mA g^{-1} in a voltage range of 0.005-2.5 V. The initial discharge and the charge capacities are found to be 581 and 205 mAh g^{-1}, respectively. The discharge capacity is decreased to ca. 300 mAh g^{-1}, but the charge capacity is still kept at 200 mAh g^{-1}. With the cycling going on, the discharge and charge capacities could be kept at about 200 mAh g^{-1} at the same current density. The large capacity loss in the initial cycles is mainly attributed to the interfacial reaction between NTO electrode and electrolyte, leading to the formation of Solid Electrolyte Interphase (SEI) film; the SEI film may be formed on both inner and outer surfaces of the NTO nanotubes. Due to the 3D spider-web architecture, plus the easy electrolyte access into the inner tube of NTO, and with the facile diffusion of Na^+ ions into the inner tube, the charge loss can be ignored in the whole cycling. Moreover, the spider web-like $Na_2Ti_3O_7$ electrode possesses a good cyclic stability at the current density of a 400 mA g^{-1} as shown in Fig. 4b. The specific discharge capacity can be kept at 200 mAh g^{-1} after 100 cycles, and the coulombic efficiency is increased from 60% at first cycle to ~100%, subsequently. Furthermore, benefiting from the special structure, the spider web-like $Na_2Ti_3O_7$ nanotube exhibits a great cycling response to a continuously varying current density rate. As shown in Fig. 4c, the as prepared $Na_2Ti_3O_7$ electrode delivers charge capacities of about 425, 250, 200, 150, 125 mAh g^{-1} with current density of 0.05, 0.1, 0.2, 0.5 and 1 A g^{-1}, respectively corresponding to 0.28C (1C corresponding to 177 mA/g), 0.56C, 1.1C, 2.8C, 5.6C, and 8.4C. When the current density is above 1 A g^{-1}, such as at the current densities of 2 and 3 A g^{-1}, the charge capacity can still be kept at 100 mAh g^{-1}, indicating the excellent rate capability of the spider web material. As shown in Fig. 4d, at a current density of 0.5 A g^{-1}, the electrode still keeps a capacity of 107 mAh g^{-1} even after 500 cycles with only ca. 28% capacity loss, and the coulombic efficiency is almost 100%, indicating that the

spider web-like $Na_2Ti_3O_7$ architecture achieved a durable cycling performance. There is no doubt that the excellent performance of the NTO electrode stems from its unique structure. For instance, the network of spider web-like electrode could act as a buffer for reducing the damage arising from the volume variation during the discharge-charge cycling. Meanwhile, the large open space of the architecture permits the electrolyte access to the whole electrode easily, facilitating the Na^+ ion transport. While the Cyclic voltammetry (CV) and EIS data are both shown in Figure S4 and S5.

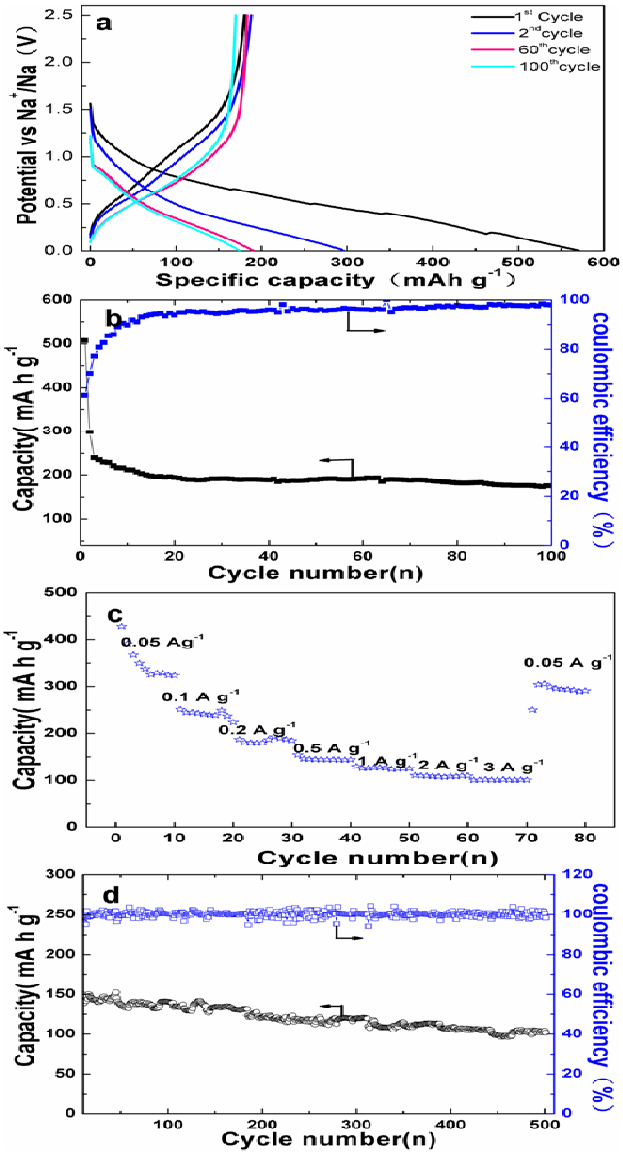

Fig. 4 a) Discharge/charge profiles in different cycles at a current density of 400 mA g^{-1}. b) Short-term cycling performance and the coulombic efficiency at a current density of 400 mA g^{-1}. c) Rate capability obtained at different current density. d) Cycling performance and coulombic efficiency at 500 mA g^{-1}.

The electrochemical sodium insertion/extraction mechanism during the discharge/charge process was studied by X-ray absorption Fine Structure (XAFS). XAFS spectra of NTO at the Ti K-edge are shown in Fig.5. As shown in Fig.5a, no obvious change were observed in the normalized Ti K-edge among initial NTO, the NTO charged to 2.5 V and the NTO discharged to 0.005 V. However, when carefully analysing the detail of the Ti pre-edge feature as shown in Fig.5b, great difference can be found out, the absorption spectrums obtained at the Ti pre-edge of initial, charged and discharged NTO were almost located at the same energy of position. While the intensity of the Ti pre-edge of the initial, charged and discharged NTO are different. Meanwhile, the partial main Ti K-edge XANES spectra of initial $Na_2Ti_3O_7$, the $Na_2Ti_3O_7$ charged to 2.5 V and the $Na_2Ti_3O_7$ discharged to 0.005V also exhibit similar change as that of the pre-edge as shown in Fig. 5c, both indicating the local coordination environment of Ti in NTO are variable as sodium insert/extract into/from the frame of $Na_2Ti_3O_7$ during the discharge/charge process. In the discharge process, the sodium atom insert into the crystal lattice, the initial crystal lattice would be distorted so as to accept more Na atoms in an equilibrium state with lowest energy, and the transition state of $Na_{2+x}Ti_3O_7$ was formed as below equation 1:

$$Na_2Ti_3O_7 + x\,Na^+ + x\,e^- = Na_{2+x}Ti_3O_7 \quad (3.5>x>0) \qquad (1)$$

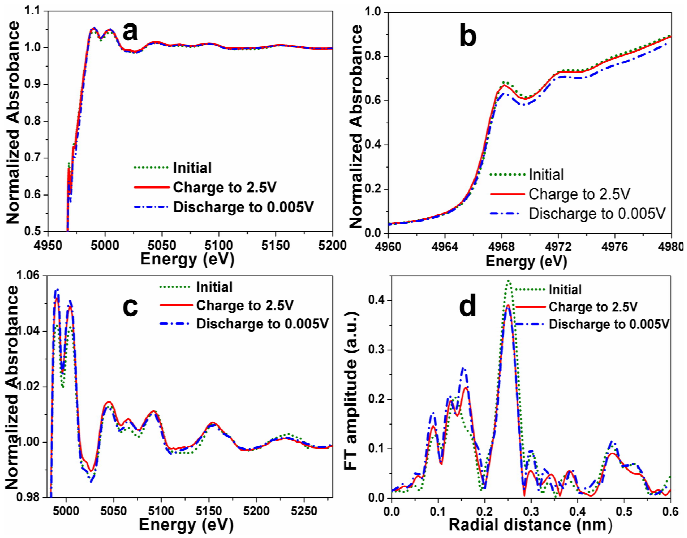

Fig. 5 Normalized Ti K-edge XAFS spectra of initial $Na_2Ti_3O_7$ electrode, the electrode charged to 2.5 V and the electrode discharge to 0.005 V. a) the whole region XAFS spectra. b) pre-edge region of XAFS. c) main-edge region of XAFS. d) Fourier transforms of Ti K-edge. (Fourier transformed but not phase corrected)

When the sodium extract from the transition state of $Na_{2+x}Ti_3O_7$ (maximum of x equal to 3.5 refer to the Reference 18 by far), the crystal lattice would also change during the charge process, due to the atoms in $Na_{2+x}Ti_3O_7$ readjust the position or reconstruct in the crystal lattice. This change can be clearly confirmed from the Fourier Transformed amplitude (FT) of Ti K-edge ex-suit XAFS of $Na_2Ti_3O_7$ with charged or discharge and without those treatments as shown in Fig. 5d.The FT amplitude peaks at 0.1-0.2 nm belong to the first neighbor O-contribution around Ti (Ti-O bond).[19] Moreover, a remarkable amplitude peak centered at 0.25 nm is ascribed to Ti-Ti bond due to the XAFS test over the NTO substrated on Ti flake. In addition, as the intensity of peak of the initial and the NTO discharged to 0.005 V here are extensively higher than that of the NTO charged to 2.5 V, really demonstrating the sodium insertion/extraction conducted during the discharge/charge processes.

It is of interest to compare the present result with those using $Na_2Ti_3O_7$ electrodes reported in the recent literature. Rudola et al. prepared NTO through a solid-state route and the $Na_2Ti_3O_7$ showed a charge capacity of 177 mAh g^{-1} at 0.1 C (0.1 C means 2 Na insertions into $Na_2Ti_3O_7$ in 10 h, corresponding to a current rate of 211 mA g^{-1}).[11] Wang et al.[12] synthesized $Na_2Ti_3O_7$ microspheres consisting of tiny nanotubes of ca. 8 nm. When the NTO microspheres were used as anode for sodium ion battery test, the discharge capacity of 108 mAh g^{-1} was maintained over 100 cycles at a current density of 354 mAg^{-1}. This group[18] also prepared single crystalline NTO rods as anode for room temperature sodium ion

battery, the discharge capacity of 103 mAh g^{-1} was only maintained over 20 cycles at a C-rate of 0.1. Chen and co-worker [10] reported NTO prepared by solid reaction delivered 188 mAh g^{-1} at a current rate of 0.1 C in a voltage of 0.0-3.0 V, but the unsatisfactory cyclic property remained to be improved. By comparison, the anode electrochemical performance, including reversible capacity, rate capability and cyclic property, of our $Na_2Ti_3O_7$ nanotube assembled 3D spider-web architecture is superior. In addition, the cell assembly in this work is also more time saving and more economical thanks to the way that the active electrode is directly formed on current collector without adding any additives.

Conclusions

We have developed an effective strategy for fabricating a spider web-like $Na_2Ti_3O_7$ nanotube electrode. Benefiting from this special structure, the electrode exhibits high reversible capacity, excellent rate capability and great long-term cycling performance at room temperature in sodium-ion battery. From the ex-suit XAFS spectra of Ti K-edge, as we expected, charging and discharging of NTO electrode in the electrolyte of Na sea were corresponding to the sodium extraction and insertion from/into the host matrix of NTO during cycling process.

This work was supported from the National Basic Research Program of China (Grant 2010CB934700).

Notes and references

[a] *School of Chemistry and Environment, Beihang University. Beijing, 100191, P. R. China. E-mail: guolin@buaa.edu.cn*

[b] *Department of Chemistry, The Hong Kong University of Science and Technology, Clear Water Bay, Kowloon Hong Kong (P.R. China). E-mail: chsyang@ust.hk*

† Electronic Supplementary Information (ESI) available: [experimental details and characterization of spider-web like NTO]. See DOI: 10.1039/c000000x/

1 N.Yabuuchi, M. Kajiyama, J.Iwatate, H. Nishikawa, S.Hitomi, R.Okuyama, R. Usui, Y. Yamada, S. Komaba, *Nat. Mater.*, 2012,**11**, 512.

2 S.W. Kim, D. H. Seo, X. Ma, G. Ceder, K. Kang, *Adv. Energy Mater.* 2012, **2**, 710; M. D. Slater, D. Kim, E. Lee, C. S. Johnson, *Adv. Funct. Mater.,* 2013, **23**,947;V. Palomares, P. Serras, I.Villaluenga, K. B.Hueso, J. Carretero-González, T. Rojo, *Energy Enviro. Sci.*, 2012, **5**, 5884.

3 S. Tepavcevic, H. Xiong, V. R. Stamenkovic, X. Zuo, M. Balasubramanian, V. B. Prakapenka, C. S. Johnson, T. Rajh, *ACS Nano,* 2011,**6**, 530; S. Komaba, T. Mikumo , A. Ogata, *Electrochem. Commun.*, 2008, **10** , 1276; S. Komaba, T. Mikumo, N. Yabuuchi, A. Ogata, H. Yoshida, Y. Yamada*, J. Electrochem. Soc.*, 2010, **157** , A60; R.E. Schaak, T. Klimczuk, M.L. Foo, R.J. Cava, *Nature*, 2003, **424**, 527.

4 P. Moreau, D. Guyomard, J. Gaubicher, F. Boucher, *Chem. Mater*., 2010, **22** ,4126; K. T. Lee, T. N. Ramesh, F. Nan, G. Botton, L. F. Nazar, *Chem. Mater.*, 2011, **23**, 3593; P. Barpanda, J. N. Chotard, N. Recham, C. Delacourt, M. Ati, L. Dupont, M. Armand, J. M. Tarascon, *Inorg. Chem.*, 2010, **49**, 7401; R. Tripathi, T. N. Ramesh, B. L. Ellis, L. F. Nazar, *Angew. Chem. Int. Ed.*, 2010, **46**, 8920.

5 Y. Lu, L. Wang, J. Cheng, J. B. Goodenough, *Chem. Commun.*, 2012, **48**, 6544; L. Wang, Y. Lu, J. Liu, M. Xu, J. Cheng, D. Zhang, J. B. Goodenough, *Angew. Chem. Int. Ed.*, 2013, **52**, 1964.

6 M. M. Doeff, Y. Ma, S. J. Visco, L. C. De Jonghe, *J. Electrochem. Soc*., 1993, **140**, L169.

7 R. Alcántara, J.M. Jiménez-Mateos, P. Lavela, J. L.Tirado, *Electrochem. Commun.*, 2001, **3** , 639.

8 X. Xia, J. R. Dahn, *J. Electrochem. Soc.*, 2012, **159**, A515.

9 P. Senguttuvan, G. Rousse, V.Seznec, J.M. Tarascon, M.R. Palacín, *Chem. Mater.*, 2011, **23**, 4109.

10 H. Pan, X. Lu, X. Yu, Y.S. Hu, H. Li, X.Q. Yang, L. Chen, *Adv. Energy Mater.*, 2013, **3**,1186.

11 A. Rudola, K. Saravanan, C. Masona, P. Balaya, *J. Mater. Chem. A*, 2013, **1**, 2653.

12 W.Wang, C.Yu, Z. Lin, J. Hou, H. Zhu, S. Jiao, *Nanoscale,* 2013, **5**, 594.

13 X. Wang, J. Ding, B. Yu, Y. Si, S.Yang, G. Sun, *Nanoscale*, 2011,**3**, 911.

14 L. Shen, E. Uchaker, X. Zhang, G. Cao, Adv. Mater., 2012, 24, 6502.

15 S. Andersson , A. D. Wadsley, *Acta Cryst.*, 1961,**14** ,1245.

16 N. Miyamoto, K. Kuroda, M. Ogawa, *J. Mater. Chem*., 2004, **14**, 165.

17 Y. An, Z. Li, H. Xiang, Y. Huang, J. Shen, *Cent. Eur. J. Phys*. 2011, **9**, 1488.

18 W. Wang, C. Yu, Y. Liu, J. Hou, H. Zhu, S. Jiao, *RSC Adv.*, 2013, **3**, 1041.

19 F. Farges, G. E. Brown Jr, J. J. Rehr, *Geochimica et Cosmochimica acta*, 1996, **60**, 3023.

